AGU PUBLICATIONS

Geophysical Research Letters

RESEARCH LETTER
10.1002/2015GL066306

Key Points:
- Morin transition temperature changes with pressure with a rate of +25 K/GPa
- The Morin transition reaches room temperature at between 1.38 and 1.61 GPa
- We quantified the effect of pressure wave on the upper crust magnetization for Earth and Mars

Supporting Information:
- Supporting Information S1

Correspondence to:
N. S. Bezaeva,
bezaeva@physics.msu.ru

Citation:
Bezaeva, N. S., F. Demory, P. Rochette, R. A. Sadykov, J. Gattacceca, T. Gabriel, and Y. Quesnel (2015), The effect of hydrostatic pressure up to 1.61 GPa on the Morin transition of hematite-bearing rocks: Implications for planetary crustal magnetization, *Geophys. Res. Lett.*, *42*, 10,188–10,196, doi:10.1002/2015GL066306.

Received 23 SEP 2015
Accepted 16 OCT 2015
Accepted article online 9 NOV 2015
Published online 12 DEC 2015

The effect of hydrostatic pressure up to 1.61 GPa on the Morin transition of hematite-bearing rocks: Implications for planetary crustal magnetization

Natalia S. Bezaeva[1,2,3], François Demory[4], Pierre Rochette[4], Ravil A. Sadykov[5], Jérôme Gattacceca[4], Thomas Gabriel[4], and Yoann Quesnel[4]

[1]Earth Physics Department, Faculty of Physics, M.V. Lomonosov Moscow State University, Moscow, Russia, [2]Institute of Physics and Technology, Ural Federal University, Ekaterinburg, Russia, [3]Institute of Geology and Petroleum Technologies, Kazan Federal University, Kazan, Russia, [4]Aix-Marseille Université, CNRS, IRD, CEREGE UM34, Aix en Provence, France, [5]Institute for Nuclear Research, Russian Academy of Sciences, Moscow, Russia

Abstract We present new experimental data on the dependence of the Morin transition temperature (T_M) on hydrostatic pressure up to 1.61 GPa, obtained on a well-characterized multidomain hematite-bearing sample from a banded iron formation. We used a nonmagnetic high-pressure cell for pressure application and a Superconducting Quantum Interference Device magnetometer to measure the isothermal remanent magnetization (IRM) under pressure on warming from 243 K to room temperature (T_0). IRM imparted at T_0 under pressure in 270 mT magnetic field (IRM_{270mT}) is not recovered after a cooling-warming cycle. Memory effect under pressure was quantified as IRM recovery decrease of 10%/GPa. T_M, determined on warming, reaches T_0 under hydrostatic pressure 1.38–1.61 GPa. The pressure dependence of T_M up to 1.61 GPa is positive and essentially linear with a slope $dT_M/dP = (25 \pm 2)$ K/GPa. This estimate is more precise than previous ones and allows quantifying the effect of a pressure wave on the upper crust magnetization, with special emphasis on Mars.

1. Introduction

Hematite (αFe_2O_3) is a common mineral in paleomagnetic and rock magnetic studies. It is abundant in both igneous and sedimentary terrestrial rocks [*Dunlop and Özdemir*, 1997] and may carry large crustal magnetization on Earth [*McEnroe et al.,* 2004; *Ouabego et al.,* 2013]. This mineral is also stable in the Martian surface conditions [*Bandfield*, 2002; *Chevrier et al.,* 2004; *Wiens et al.,* 2015], and it has been proposed as a candidate magnetic mineral for the Martian magnetic anomalies [*Dunlop and Kletetschka*, 2001]. However, Martian meteorites point more toward sulfide or spinel oxide [*Rochette et al.,* 2005; *Gattacceca et al.,* 2014], although the occurrence of hematite is also reported [*McCubbin et al.,* 2009].

Hematite is essentially antiferromagnetic with a superimposed weak ferromagnetism at room pressure and temperature. Hematite is characterized by the so-called Morin transition [*Morin*, 1950]. This is a first-order magnetic phase transition (temperature-driven spin-flop) from a weakly ferromagnetic to antiferromagnetic state, which occurs on cooling below $T_M \sim 250$ K [*Morin*, 1950; *Bowles et al.,* 2010]. The transition occurs on warming above T_M, although there is a thermal hysteresis and T_M temperatures on cooling and on warming may be different [*Özdemir et al.,* 2008].

The Morin transition was shown to be sensitive to the effects of grain size [*Özdemir et al.,* 2008], impurities [*Morin*, 1950; *Besser and Morrish*, 1964], grinding, and shocks [*Williamson et al.,* 1986] as well as static pressures (see Table S1 in the supporting information for references). Pressure dependence of Morin transition has been previously investigated theoretically [*Searle*, 1967; *Allen*, 1973] as well as through a wide range of experimental techniques such as nuclear magnetic resonance experiments [*Wayne and Anderson*, 1967], neutron scattering [*Umebayashi et al.,* 1966; *Worlton et al.,* 1967; *Goncharenko et al.,* 1995; *Parise et al.,* 2006; *Klotz et al.,* 2013], Mössbauer studies [*Vaughan and Drickamer*, 1967; *Bruzzone and Ingalls*, 1983], and static magnetic measurements [*Kawai and Ono*, 1966]. It was established that T_M increases with increasing pressure (Table S1), contrary to the Verwey transition temperature of magnetite that decreases with increasing hydrostatic pressure with a rate of the order of −3 K/GPa [*Coe et al.,* 2012; *Sato et al.,* 2012].

Different estimates of pressure sensitivity of T_M (dT_M/dP) are summarized in Table S1. As follows from Table S1, previous experimental studies were limited to either low-pressure range [*Kawai and Ono*, 1966; *Umebayashi et al.,* 1966; *Wayne and Anderson*, 1967], nonhydrostatic conditions [*Parise et al.,* 2006; *Goncharenko et al.,* 1995], or indirect (i.e., nonmagnetic) measurements [*Worlton et al.,* 1967; *Klotz et al.,* 2013]. Moreover, there is still no consensus in literature (Table S1) about the pressure at which the Morin transition reaches room temperature (T_0). Indeed, *Searle* [1967] and *Parise et al.* [2006] predicted the Morin transition to reach T_0 at about 1.5 GPa and 10 GPa, respectively; *Vaughan and Drickamer* [1967] claimed to have observed a pressure-induced Morin transition at T_0 under 3 GPa, whereas *Worlton and Decker* [1968] showed that at T_0 the Morin point does not vary with pressure above 2.5 GPa. *Klotz et al.* [2013] reported that the T_M reaches T_0 at about 1.5–1.7 GPa and moves beyond T_0 at higher pressures [see *Klotz et al.,* 2013, Figure 3 wherein].

It was previously reported that the behavior of hematite under high pressure is markedly different in different pressure media [*Parise et al.,* 2006; *Klotz et al.,* 2013]. *Klotz et al.* [2013] argue that the conclusions drawn from nonhydrostatic measurements of the Morin transition under pressure are most likely unreliable. Pressure sensitivity of T_M reported in Table S1 varies between 10 and 100 K/GPa, a range unlikely to represent real variability rather than poor definition of the experimental parameters. In addition, hydrostatic experiments may represent a better analog for natural in situ conditions [*Demory et al.,* 2013]. It is known that lithostatic pressure at 50 km depth is about 1.5 GPa on Earth. On the other hand, Mars shows a pressure gradient of 1.5 GPa per 100 km, and the Martian crustal magnetization may be carried on a thick section of the crust up to 50 km [*Langlais et al.,* 2004]. Thus, the most relevant hydrostatic pressure range for terrestrial and Martian crustal conditions is limited to 1.5 GPa. However, previous authors have not investigated this pressure range in details. Indeed, *Klotz et al.* [2013] and *Worlton et al.* [1967] provide for this pressure range only two and three data points of T_M versus pressure, respectively.

Moreover, in spite of previous efforts, direct magnetic measurements of T_M pressure dependence performed on hematite-bearing rocks under hydrostatic conditions up to 1.5 GPa are still lacking. Such work may have implications for further modeling of crustal magnetic anomalies. On the other hand, if we consider the average temperature gradients on Earth and Mars (20 K/km and 6–10 K/km, respectively [*Hoffman*, 2001; *Clifford et al.,* 2010]), standard dT/dP on Earth and Mars crustal depth profile are 700–1000 K/GPa and 400–700 K/GPa, respectively. This implies that under normal conditions, the pressure dependence of T_M has only a second-order effect on the magnetic state of hematite versus depth. Only temporary pressure increases due to shock waves can lead to an interesting situation that will be discussed forward later for the Martian case, where surface temperatures vary from $<$200 K to ~285 K [*Martinez et al.,* 2014] and the average equatorial surface temperature is about 220 K [*Hoffman*, 2001].

We present here new magnetic data on the hydrostatic pressure dependence of the Morin transition up to 1.61 GPa obtained on a well-characterized multidomain (MD) hematite-bearing rock sample from banded iron formation, which is possibly responsible for the largest large-scale magnetic anomaly on Earth [*Demory et al.,* 2013; *Ouabego et al.,* 2013]. We used a nonmagnetic high-pressure cell of piston-cylinder type for hydrostatic pressure application and a Superconducting Quantum Interference Device (SQUID) magnetometer for remanent magnetization measurements under pressure in the course of zero-field warming of the cell with sample from 243 K to T_0. Thus, we report here the Morin transition temperature T_M under pressure determined on warming.

2. Samples and Measuring Techniques

2.1. Description of Samples

We selected a MD hematite-bearing sample from a banded iron formation sampled from Centrafrican Republic, previously characterized by *Ouabego et al.* [2013] and *Demory et al.* [2013] (sample ID: BG8603). Pure hematite was confirmed by a large Morin transition and typical hysteresis properties, using a Princeton Micromag vibrating sample magnetometer (VSM). Morin temperature was determined to be 255 K, based on cycling in a 0.2 T field. The sample has the following hysteresis parameters: coercivity $B_c = 21.9$ mT, coercivity of remanence $B_{cr} = 28.5$ mT, saturation isothermal remanent magnetization $M_{rs} = 55$ mA m^2/kg and saturation magnetization $M_s = 109$ mA m^2/kg [*Ouabego et al.,* 2013].

Isothermal remanent magnetization (IRM) acquisition curves up to 1 T, acquired in three perpendicular directions at ambient pressure and temperature (Figure S3b), confirmed that IRM_{270mT} (see below) may be

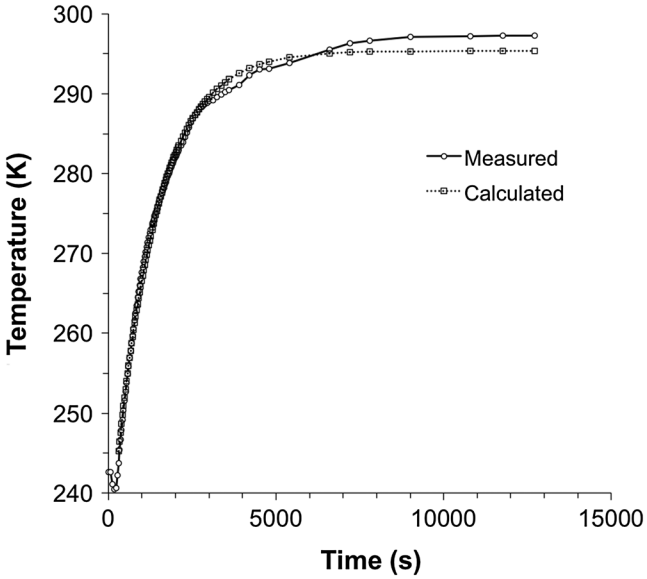

Figure 1. Temperature inside the teflon capsule of the pressure cell as a function of time. Both measured (solid line) and modeled (dashed line) temperatures are shown.

considered as a reasonable analog for SIRM (saturation IRM). Indeed, IRM_{270mT} represents 96–98% of SIRM (Figure S3b).

2.2. Experimental Protocol and Measurements

All processes and measurements described below were carried out at CEREGE (Aix-en-Provence, France).

The sample was pressurized using a nonmagnetic high-pressure clamp cell of piston-cylinder type allowing direct measurement in a SQUID magnetometer. This cell presents several modifications with regard to the cell described by *Sadykov et al.* [2008]. First, this new cell was entirely made of "Russian alloy" ($Ni_{57}Cr_{40}Al_3$) as the cell described by *Sadykov et al.* [2009]. Second, its inner diameter is 7 mm, and the maximum calibrated pressure is 2.0 GPa. The actual pressure at room temperature is about 10% less than the pressure estimated from the known external load [*Sadykov et al.,* 2008] (additionally, for the temperature range below room temperature, pressure values presented in Figures 2, 3 and S2 were corrected for ΔP, calculated according to equation (1) below, see section 3.2). We used the following protocol for all measurements of magnetic remanence under pressure from 243 K to room temperature. The sample was placed into a teflon capsule, filled with inert polyethylsiloxane (PES-1) liquid and locked with a teflon plug. PES-1 allows converting the uniaxial pressure on the pistons into a pure hydrostatic pressure [*Kirichenko et al.,* 2005]. After loading of the cell with a press (Graseby Specac 15011), the pressure inside the cell was locked. Pressure loading always occurred within a magnetically shielded room (ambient field ~100 nT) at T_0. Sample inside the pressure cell was then placed in a 270 mT magnetic field to acquire IRM (further referred to as IRM_{270mT}) following the same procedure as described in *Demory et al.* [2013]. The cell was then placed into freezer and kept at 243 K for about 10 h before starting the remanence measurement. An isotherm box was used to prevent the cell from warming during the transport from the freezer to the magnetometer, which took on average 5 min (150 m). The magnetic moment of the sample under pressure was then measured using a 2G Enterprises SQUID magnetometer. This magnetometer allows for the measurement of magnetic moments up to 10^{-4} A m^2 with a practical background noise level of 10^{-11} A m^2. The protocol (including IRM acquisition step) was repeated for each of subsequent pressure steps up to 1.38 GPa and 1.61 GPa during two independent runs of loading. We also conducted in the same manner one cooling-warming cycle using empty pressure cell (with no sample) at zero pressure; its IRM varies within 6–7% from IRM_{270mT} at zero pressure for the full temperature range (Figures 2 and S4).

Time was monitored continuously from the moment of pressure cell removal from the freezer. Delay between two remanence measurements was ~2.0–2.5 min. By replacing the sample by a thermocouple in the cell, we constructed a temperature versus time model (see section 3.1 and Figure 1). The Morin transition temperature T_M was determined as the maximum in the first derivative of remanence warming curve (in accordance with *Feinberg et al.* [2015]). The T_M value determined in this way at atmospheric pressure is in accordance with *Özdemir et al.* [2008], who indicated T_M ranging from 250 K to 261 K for 0.5–6 mm hematite natural single crystals and from 257 K to 260 K for 45–600 μm sieved crystal fractions. In this work we did not aim to investigate the defect moment of hematite [*Özdemir and Dunlop*, 2006] nor its pressure sensitivity. IRM acquisition curves (Figure S3b) in three perpendicular directions and a major hysteresis loop (Figure S3a) were acquired using a Princeton Micromag VSM with maximum applied magnetic field of 1 T.

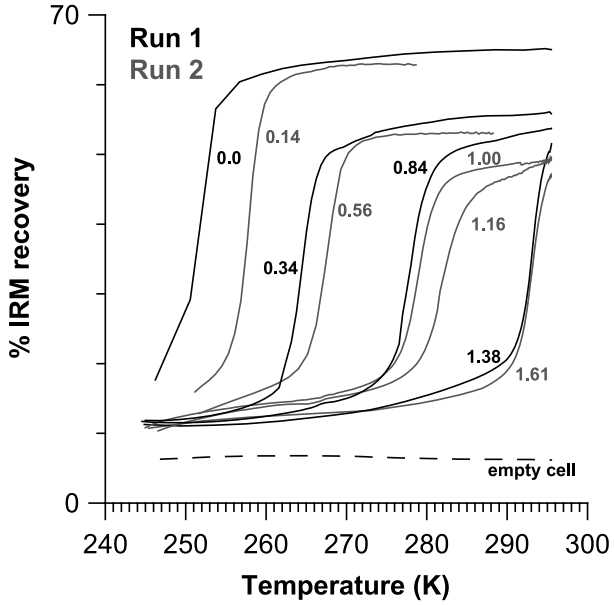

Figure 2. IRM recovery under pressure versus temperature measured on warming. Pressure values, indicated next to each curve, are in GPa and correspond to pressures at the Morin transition temperature. IRM recovery values are normalized by IRM_{270mT} at T_0 and are presented in percents. IRM recovery of empty cell is normalized by IRM_{270mT} at zero pressure.

3. Experimental Results

3.1. Time-Temperature Intercalibration

Warming of the cell in direct contact with the laboratory atmosphere was monitored using a thermocouple, which was placed inside the teflon capsule of the pressure cell in lieu of the sample, and a chronometer. We fit this time-temperature data set with a simple conductive warming model, using the equation $T = T_f + (T_i - T_f)\, e^{-at}$, where T_f is the final temperature (room temperature 295.4 K), T_i is the initial temperature (245.2 K), t is the time, and a is a coefficient depending (among other things) on the heat capacity of the cell. The best fit is obtained for $a = 8.0384 \times 10^{-4}$ (Figure 1). In the following we use the calculated curve to convert the measured time into temperature. It appears that the model is robust up to 288 K (actual difference between the measurement and the calculation at every t is $\leq$1 K).

3.2. Pressure-Temperature Intercalibration

Cooling the pressure cell with the sample down to 243 K resulted in a pressure decrease ΔP within the sample chamber due to different thermal expansion coefficients of the pressure cell body material (Russian alloy) and liquid pressure medium (PES-1). ΔP was calculated as following under assumption of incompressibility of the sample and neglecting teflon vessel:

$$\Delta P = -\frac{\Delta T}{\beta}\left[\alpha^*\left(1 + \frac{V_s}{V_L}\right) - \alpha\right] \quad (1)$$

where $\Delta T = T_2 - T_1$; T_1 and T_2 (in K) are T_0 and a temperature from 243 K to 293 K range, respectively; α and α^* are volume thermal expansion coefficients (in 1/K) of PES-1 and Russian alloy, respectively; β is coefficient of volume compressibility of PES-1; V_S is sample volume, and V_L is PES-1 volume. $\alpha \sim 8.5 \cdot 10^{-4}$ 1/K. α^* for Russian alloy is $31.5 \cdot 10^{-6}$ 1/K ($T = 293$ K) and $30.0 \cdot 10^{-6}$ 1/K ($T = 243$ K); it was calculated using the chemical composition of Russian alloy (wt %: $Ni_{57}Cr_{40}Al_3$) and linear thermal expansion coefficients of Ni, Cr, and Al for different temperatures [*Grygoriev and Meilikhov,* 1991] and under assumption of isotropy of NiCrAl. These calculated values are in accordance with our experimental data on linear thermal expansion coefficient for NiCrAl at $T = 298$ K and two perpendicular directions: $(10.94 \pm 0.05) \cdot 10^{-6}$ 1/K and $(10.32 \pm 0.05) \cdot 10^{-6}$ 1/K, respectively. $\alpha^*(T)$ was calculated based on equation expressing linear fit between α^*(293 K) and α^*(243 K). $\beta(P)$ for PES-1 was supposed to be the same as for PES-2 liquid medium at $T = 303$ K, which was taken from *Kagramanyan* [1984] for 0.23 GPa, 0.46 GPa, and up to 0.60 GPa, the latter was further extrapolated to 1.61 GPa, by assuming a saturation effect. $\beta = 0.304$ GPa^{-1} (for 0.23 GPa), $\beta = 0.192$ GPa^{-1} (for 0.46 GPa), $\beta = 0.157$ GPa^{-1} for $T = 303$ K, $P \in [0.6; 1.61]$ GPa. It was also assumed that β does not change within the given temperature range [243 K; 303 K]. It is important to mention that experimental data on $\beta(P)$ for PES-2 and PES-3 are almost identical [*Kagramanyan*, 1984]. V_S was calculated from sample's dimensions, and V_L was calculated from the cell's geometry. In this work $V_S \sim V_L/9$.

Figure S1 displays pressure-temperature dependences for initial (room temperature) pressures $P_1 = 0.23$ GPa, $P_2 = 0.46$ GPa, and $P_3 \in [0.6; 1.61]$ GPa. Maximum initial pressure of 1.61 GPa is obtained at 293 K. All pressure values for $T < T_0$ in Figures 2, 3 and S2 were corrected for ΔP using data from Figure S1.

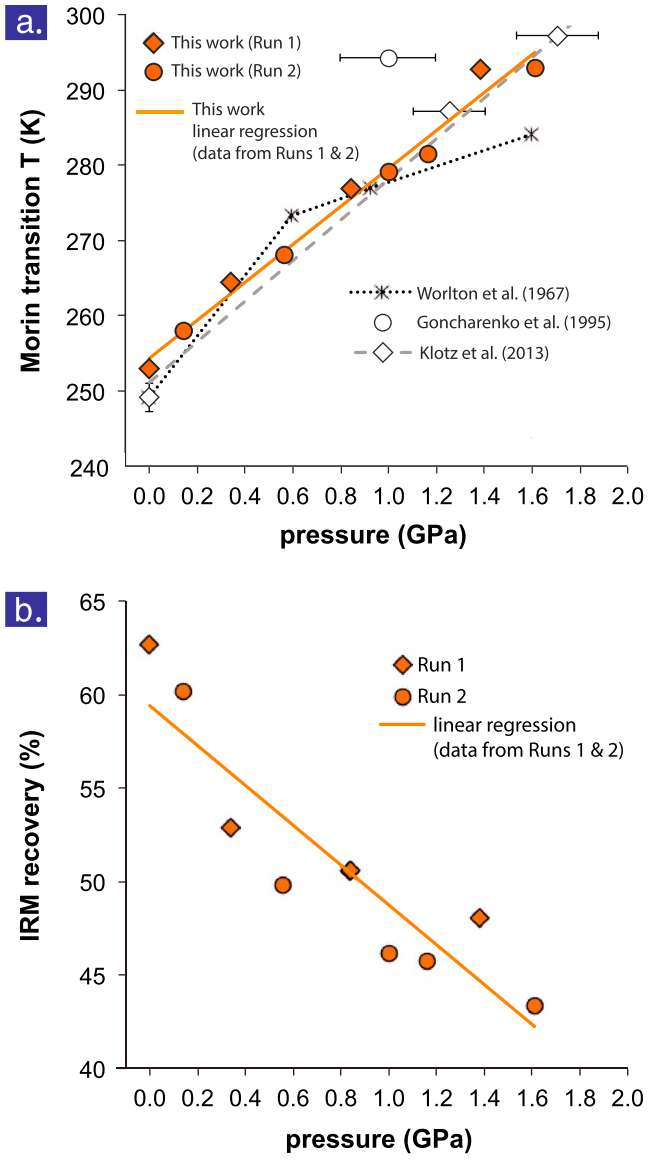

Figure 3. (a) The Morin transition temperature under pressure up to 1.61 GPa (this work) and up to 2.0 GPa (previous studies: [*Worlton et al.,* 1967; *Goncharenko et al.,* 1995; *Klotz et al.,* 2013]). Solid line corresponds to linear regression for data points from both data sets (Runs 1 and 2) with approximation confidence $R^2 = 0.98$ ($y = ax + b$, where $a = 25.23$ and $b = 254.37$); gray dashed line corresponds to linear fit for all data points presented in Figure 3 of *Klotz et al.* [2013] up to 4 GPa pressure range (only three data points from this figure are presented here); (b) percent of recovered IRM (with regard to IRM_{270mT}, imparted under pressure at room temperature) versus hydrostatic pressure up to 1.61 GPa. Both IRM and IRM_{270mT} were corrected for IRM of empty cell (Figure S4). Solid line corresponds to linear regression for data points from both data sets (Runs 1 and 2) with approximation confidence $R^2 = 0.83$ ($y = ax + b$, where $a = -10.65$ and $b = 59.40$).

3.3. Morin Transition Under Pressure and Repeatability of Our Experiments

We conducted two independent pressure runs with the following initial pressure steps (in GPa): (first run) 0, 0.46, 0.92, and 1.38 and (second run) 0.23, 0.69, 1.08, 1.22, and 1.61. IRM recovery values (normalized by room temperature IRM_{270mT}) versus temperature under pressure are presented in Figure 2. Actual pressure is dependent on temperature and varies within the presented temperature range (Figure S1). Pressures indicated in Figures 2 and S2 correspond to $P(T_M)$ values.

Figure 2 confirms that T_M increases gradually with increasing pressure, consistent with previous studies (Table S1). The Morin transition width extracted from full width at half maximum of the dIRM/dT is $\leq$6 K in all pressure range. IRM is never completely recovered after warming (Figure 2) due to well-documented memory effect after a cooling-warming cycle through T_M [*Kletetschka and Wasilewski,* 2002; *Özdemir and Dunlop,* 2006]. The percentage of IRM recovery with regard to initial room temperature IRM_{270mT} under pressure (memory ratio) decreases with increasing pressure (Figure 3b).

The repeatability of warming cycles was tested for 0.14 GPa and 0.56 GPa pressures (Figure S2). As seen from repetitive warming cycles of IRM versus temperature (Figure S2), the thermal experiments are repeatable with a slight difference of less than 2 K.

4. Discussion

Figure 3 displays the Morin transition temperature T_M (Figure 3a) and the percentage of IRM recovery after a cooling-warming cycle with regard to IRM_{270mT} (Figure 3b) under hydrostatic pressure up to 1.61 GPa. The data are also summarized in Table S2.

Pressure dependence of T_M is mostly linear. T_M reaches room temperature under hydrostatic pressure of 1.38–1.61 GPa, which is consistent with predictions of *Searle* [1967] and *Allen* [1973] and at odds with predictions of *Parise et al.* [2006]. Indeed, in spite of hydrostatic conditions up to ~2.3 GPa [*Sidorov and Sadykov,* 2005] *Parise et al.* [2006] did not observe the Morin transition under 1.5 GPa. This is most likely due to the

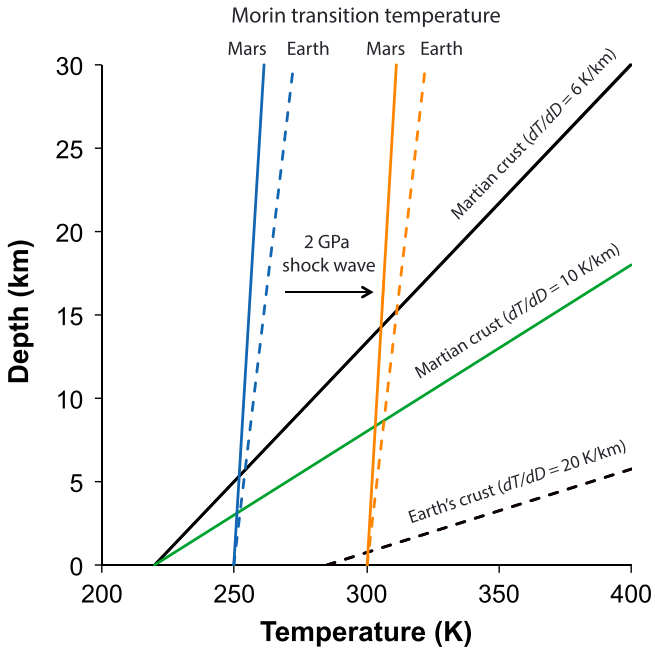

Figure 4. Crustal depth versus temperature models for Mars (solid line) and Earth (dashed line) (geothermal gradients d*T*/d*D* and surface temperatures chosen for Mars and Earth are 6 K/km, 10 K/km, and 220 K as well as 20 K/km and 285 K, respectively) compared to the Morin temperature depth dependence (Mars and Earth cases are in solid line and dashed line, respectively). The displaced Morin lines correspond to a 2 GPa isothermal pressure increase. *D* is crustal depth.

uncertainly in T_M determination. It may also be related to the usage of a different experimental technique and/or a hematite sample with different grain size (20–50 nm sized powder).

In the study of *Goncharenko et al.* [1995], where the Morin transition was not reached at T_0 under 10 GPa, it is likely due to nonhydrostatic environment. Indeed, *Goncharenko et al.* [1995] did not use any pressure transmitting medium at all, and it is known that small areas of nonuniform stress can make large changes in crystalline anisotropy of parts of the sample [*Dunlop and Özdemir*, 1997].

Our experimental data allow estimating the pressure sensitivity of T_M as 25 ± 2 K/GPa (Figure 3a). This pressure dependence is somewhat lower than what was previously proposed for the <0.6 GPa pressure range [*Kawai and Ono*, 1966; *Umebayashi et al.,* 1966; *Wayne and Anderson*, 1967; *Worlton et al.,* 1967] but higher than what was proposed for the >0.6 GPa pressure range [*Worlton et al.,* 1967] (see Table S1). Our T_M pressure dependence is roughly consistent with the T_M pressure dependence from *Klotz et al.* [2013]; moreover, *Klotz et al.* [2013] demonstrated that it holds as well for higher pressures up to 4 GPa. We do not observe any changes in pressure sensitivity of T_M above 0.6 GPa, in accordance with the results of *Klotz et al.* [2013] and in sharp contradiction with previous authors (see Table S1 for references), which is likely to be due to nonhydrostatic pressure conditions. Our confirmation of linear trend of T_M versus pressure and estimated pressure dependence of T_M are more robust and accurate with regard to previous works due to two reasons. First, our experimental technique represents direct magnetic measurements performed using a high-sensitivity magnetometer, and with our pressure cell, the pressure application uncertainty is only below 5%. Second, we used a larger data set (nine data points versus two to three data points in previous works [*Worlton et al.,* 1967; *Klotz et al.,* 2013]) for T_M pressure sensitivity estimates in 0 to 1.61 GPa range.

Data presented in Figure 3b allows quantifying the memory effect after a cooling-warming cycle and its dependence on pressure via linear regression of all data points (Runs 1 and 2). Indeed, there is 59% of IRM recovery (with regard to initial IRM_{270mT}) observed after a cooling-warming cycle at ambient pressure. Under pressure an extra loss of 10%/GPa is observed (Figure 3b). This does not represent the "classic" isothermal pressure demagnetization [*Bezaeva et al.,* 2007, 2010] as the postcycle IRM was normalized to initial IRM_{270mT} imparted after pressurization.

It is important to mention that contrary to all previous authors (see Table S1), we used in our work a natural hematite-bearing rock sample, which is more representative of crustal materials than synthetic powders of hematite and provides a better point of comparison with natural conditions.

How does these results can help to understand the nature of crustal magnetism and planetary magnetic anomalies? Knowing the behavior of hematite in different pressure-temperature conditions allows geological mapping of magnetic anomalies of hematite-rich surfaces such as Bangui magnetic anomaly in Central African Republic [*Ouabego et al.,* 2013]. As shown here, T_M reaches room temperature at ~1.5 GPa. The temperature in the Earth's crust interiors is far above [250 K; T_0] interval. This allows assuming that hematite present in Earth's crust is in its ferromagnetic state everywhere in the crust

where the corresponding temperature does not exceed hematite's Curie temperature of 948 K [*Dunlop and Özdemir,* 1997].

Let us now consider the case of Mars and Martian magnetic anomalies. The Martian crustal magnetization is thought to be carried within a section of the crust up to 40–50 km thick [*Langlais et al.,* 2004]. Figure 4 represents the *P*/*T* situation in normal present-day conditions at the equator within the Martian crust. Depending on the chosen temperature gradient, the first 3 to 5 km of the crust are below T_M, i.e., should have reduced remanence in case hematite is the carrier. Taking into account the pressure dependence of T_M increases this thickness by only 4 to 6%.

On the other hand, in case of a major hypervelocity impact, a transient pressure increase of several GPa can affect the whole crust thickness on a planetary scale: indeed, *Hood et al.* [2003] estimate that a 2 GPa pressure threshold was exceeded up to 3000 km from the Hellas impact on Mars. Such pressure increases, resulting in a 50 K increase of T_M, will result in a farther 5 to 8 km of crust to temporarily pass below the Morin transition (note that we neglect the shock wave temperature increase generated; at 2 GPa this increase is of a few Kelvins only [e.g., *Stöffler et al*., 1991]). This results in an additional demagnetization, with respect to the usually considered pressure demagnetization effect [*Bezaeva et al.,* 2007, 2010]. In case this situation occurs in the presence of an ambient field a remagnetization linked to cycling through T_M may also occur. Therefore, this process seems significant for the modeling of the impact demagnetization of the Martian crust in case of hematite being the remanence-carrying mineral. In the case of the Earth (Figure 4) only the first kilometers of crust may be affected by the same process with a 2 GPa pressure wave. Note that this effect may also affect pressure demagnetization experiments conducted at room temperature for pressure above 1.5 GPa, possibly explaining the peculiar sensitivity to pressure demagnetization observed for hematite-bearing rocks [*Bezaeva et al.,* 2010; *Jiang et al.,* 2013]. However, one has to bear in mind nonhydrostatic (deviatoric) stress effects, relevant for shock waves, that may severely affect the pressure sensitivity of the Morin transition, as observed in the Verwey case [*Coe et al.,* 2012]. Indeed, the propagation of shock waves during impact-cratering processes produces high directional (uniaxial) stresses in shock-compressed materials, which remain in situ (and not melted); at the same time areas around and below the center of an impact crater's epicenter will also experience short-lived high hydrostatic stresses [*Pearce and Karson*, 1981], which justifies the analogy of treating the passage of a shock wave in terms of an hydrostatic pressure approach. Our conclusions from Figure 4 would remain, qualitatively, even if the actual pressure dependence of T_M would be significantly different in the shock wave conditions with respect to the experimental conditions.

5. Conclusions

1. We characterized experimentally the Morin transition of natural MD hematite-bearing rock under hydrostatic pressure up to 1.61 GPa using a nonmagnetic high-pressure cell of piston-cylinder type and a SQUID magnetometer for remanent magnetization measurements under pressure during zero-field warming of the cell with sample from 243 K to room temperature.
2. The ambient pressure cooling-warming cycle resulted in a 41% loss in IRM (with regard to IRM_{270mT}). Under pressure an extra loss of 10%/GPa is observed.
3. The Morin transition temperature T_M, determined on warming, reaches room temperature under hydrostatic pressure 1.38–1.61 GPa, consistent with theoretical predictions [*Searle*, 1967; *Allen*, 1973].
4. Pressure dependence of T_M up to 1.61 GPa is linear and positive (approximation confidence $R^2 = 0.98$), $dT_M/dP = 25 \pm 2$ K/GPa. We did not observe any changes in the pressure sensitivity of T_M above 0.6 GPa, which is consistent with *Klotz et al.* [2013]. Linear trend of T_M versus pressure in the 0 to 1.61 GPa pressure range and dT_M/dP value are confirmed more robustly and accurately than in previous works due to a much larger data set and the chosen method of direct magnetic measurements.
5. The determined pressure dependence implies that during a transient pressure increase due to shock, a significant proportion of the upper crust (especially in the Martian case) can pass through the Morin transition, leading to an extra demagnetization or remagnetization effect, not previously taken into account.

Acknowledgments
We are grateful to Mike Fuller (University of Hawai'i at Mānoa, USA) and an anonymous referee for helpful reviews. The work is performed according to the Russian Government Program of Competitive Growth of Kazan Federal University. Supporting data are included as four figures and two tables in the supporting information; any additional data may be obtained from N.S.B. (email: bezaeva@physics.msu.ru).

References

Allen, J. W. (1973), Stress dependence and the latent heat of the Morin transition in α-Fe_2O_3, *Phys. Rev. B*, *8*(7), 3224–3228.
Bandfield, J. L. (2002), Global mineral distribution on Mars, *J. Geophys. Res.*, *107*(E6), 5042, doi:10.1029/2001JE001510.
Besser, P. J., and A. H. Morrish (1964), Spin flopping in synthetic hematite crystals, *Phys. Lett.*, *13*(4), 289–290.

Bezaeva, N. S., P. Rochette, J. Gattacceca, R. A. Sadykov, and V. I. Trukhin (2007), Pressure demagnetization of the Martian crust: Ground truth from SNC meteorites, *Geophys. Res. Lett.*, *34*, L23202, doi:10.1029/2007GL031501.

Bezaeva, N. S., J. Gattacceca, P. Rochette, R. A. Sadykov, and V. I. Trukhin (2010), Demagnetization of terrestrial and extraterrestrial rocks under hydrostatic pressure up to 1.2 GPa, *Phys. Earth Planet. Inter.*, *179*, 7–20, doi:10.1016/j.pepi.2010.01.004.

Bowles, J., M. Jackson, and S. K. Banerjee (2010), Interpretation of low-temperature data. Part II: The hematite Morin transition, *IRM Q.*, *20*(1), 1, 8–10.

Bruzzone, C. L., and R. Ingalls (1983), Mossbauer-effect study of the Morin transition and atomic positions in hematite under pressure, *Phys. Rev. B*, *28*(5), 2430–2440.

Chevrier, V., P. Rochette, P. E. Mathé, and O. Grauby (2004), Weathering of iron rich phases in simulated Martian atmospheres, *Geology*, *32*, 1033–1036.

Clifford, S. M., J. Lasue, E. Heggy, J. Boisson, P. McGovern, and M. D. Max (2010), Depth of the Martian cryosphere: Revised estimates and implications for the existence and detection of subpermafrost groundwater, *J. Geophys. Res.*, *115*, E07001, doi:10.1029/2009JE003462.

Coe, R. S., R. Egli, S. A. Gilder, and J. P. Wright (2012), The thermodynamic effect of nonhydrostatic stress on the Verwey transition, *Earth Planet. Sci. Lett.*, *319*, 207–217, doi:10.1016/j.epsl.2011.11.021.

Demory, F., P. Rochette, J. Gattacceca, T. Gabriel, and N. S. Bezaeva (2013), Remanent magnetization and coercivity of rocks under hydrostatic pressure up to 1.4 GPa, *Geophys. Res. Lett.*, *40*, 3858–3862, doi:10.1002/grl.50763.

Dunlop, D. J., and G. Kletetschka (2001), Multidomain hematite: A source of planetary magnetic anomalies?, *Geophys. Res. Lett.*, *28*(17), 3345–3348, doi:10.1029/2001GL013125.

Dunlop, D. J., and Ö. Özdemir (1997), *Rock Magnetism, Fundamentals and Frontiers*, 573 pp., Cambridge Univ. Press, Cambridge, U. K.

Feinberg, J. M., P. Solheid, N. Swanson-Hysell, M. Jackson, and J. Bowles (2015), Full vector low-temperature magnetic measurements of geologic materials, *Geochem. Geophys. Geosyst.*, *16*, 301–314, doi:10.1002/2014GC005591.

Gattacceca, J., P. Rochette, R. B. Scorzelli, P. Munayco, C. Agee, Y. Quesnel, C. Cournede, and J. Geissman (2014), Martian meteorites and Martian magnetic anomalies: A new perspective from NWA 7034, *Geophys. Res. Lett.*, *41*, 4859–4864, doi:10.1002/2014GL060464.

Goncharenko, I. N., J.-M. Mignot, G. Andre, O. A. Lavrova, I. Mirebeau, and V. A. Somenkov (1995), Neutron diffraction studies of magnetic structure and phase transitions at very high pressures, *High Pressure Res.*, *14*, 41–53.

Grygoriev, I. S., and E. Z. Meilikhov (1991), *Handbook of Physical Constants*, 1232 pp., Energoatomizdat, Moscow.

Hoffman, N. (2001), Modern geothermal gradients on Mars and implications for subsurface liquids Abstract 7044 presented at the Conference on the Geophysical Detection of Subsurface Water on Mars, Lunar and Planet. Instit., Houston, Tex.

Hood, L. L., N. C. Richmond, E. Pierazzo, and P. Rochette (2003), Distribution of crustal magnetic fields on Mars: Shock effects of basin-forming impacts, *Geophys. Res. Lett.*, *30*(6), 1281, doi:10.1029/2002GL016657.

Jiang, Z., P. Rochette, L. Qingsong, J. Gattacceca, Y. Yu, V. Barron, and J. Torrent (2013), Pressure demagnetization of Al substituted hematite and its implications for planetary studies, *Phys. Earth Planet. Inter.*, *224*, 1–10, doi:10.1016/j.pepi.2013.09.005.

Kagramanyan, L. S. (1984), Elastic and thermodynamic properties of a series of silicone fluids at pressures of up to 600 MPa from acoustic measurements, PhD thesis, Yerevan Polytech. Inst., Yerevan.

Kawai, N., and F. Ono (1966), Effect of hydrostatic pressure on Morin transition point of α-hematite crystal, *Phys. Lett.*, *21*, 279.

Kirichenko, A. S., A. V. Kornilov, and V. M. Pudalov (2005), Properties of polyethylsiloxane as a pressure-transmitting medium, *Instrum. Exp. Tech.*, *48*(6), 813–816, doi:10.1007/s10786-005-0144-5.

Kletetschka, G., and P. Wasilewski (2002), Grain size limit for SD hematite, *Phys. Earth Planet. Inter.*, *129*, 173–179.

Klotz, S., T. Strassle, and T. Hansen (2013), Pressure dependence of Morin transition in α-Fe2O3 hematite, *Europhys. Lett.*, *104*, 16001, doi:10.1209/0295-5075/104/16001.

Langlais, B., M. E. Purucker, and M. Mandea (2004), Crustal magnetic fields of Mars, *J. Geophys. Res.*, *109*, E02008, doi:10.1029/2003JE002048.

Martinez, G. M., et al. (2014), Surface energy budget and thermal inertia at Gale Crater: Calculations from ground-based measurements, *J. Geophys. Res. Planets*, *119*, 1822–1838, doi:10.1002/2014JE004618.

McCubbin, F. M., N. J. Tosca, A. Smirnov, H. Nekvasil, A. Steele, M. Fries, and D. H. Lindsley (2009), Hydrothermal jarosite and hematite in a pyroxene-hosted melt inclusion in Martian meteorite Miller Range (MIL) 03346: Implications for magmatic-hydrothermal fluids on Mars, *Geochim. Cosmochim. Acta*, *73*, 4907–4917.

McEnroe, S. A., F. Langenhorst, P. Robinson, G. Bromiley, and C. Shaw (2004), What's magnetic in the lower crust?, *Earth Planet. Sci. Lett.*, *226*, 175–192.

Morin, F. J. (1950), Magnetic susceptibility of αFe_2O_3 and αFe_2O_3 with added titanium, *Phys. Rev.*, *78*, 819–820.

Ouabego, M., Y. Quesnel, P. Rochette, F. Demory, E. M. Fozing, T. Njanko, J.-C. Hippolyte, and P. Affaton (2013), Rock magnetic investigation of possible sources of the Bangui magnetic anomaly, *Phys. Earth Planet. Inter.*, *224*, 11–20, doi:10.1016/j.pepi.2013.09.003.

Özdemir, O., and D. Dunlop (2006), Magnetic memory and coupling between spin-canted and defect magnetism in hematite, *J. Geophys. Res.*, *111*, B12S03, doi:10.1029/2006JB004555.

Özdemir, O., D. Dunlop, and T. S. Berquó (2008), Morin transition in hematite: Size dependence and thermal hysteresis, *Geochem. Geophys. Geosyst.*, *9*, Q10Z01, doi:10.1029/2008GC002110.

Parise, J. B., D. R. Locke, C. A. Tulk, I. Swainson, and L. Cranswick (2006), The effect of pressure on the Morin transition in hematite (α-Fe_2O_3), *Phys. B*, *385-386*, 391–393.

Pearce, G. W., and J. A. Karson (1981), On pressure demagnetization, *Geophys. Res. Lett.*, *8*(7), 725–728, doi:10.1029/GL008i007p00725.

Rochette, P., J. Gattacceca, V. Chevrier, V. Hoffmann, J.-P. Lorand, M. Funaki, and R. Hochleitner (2005), Matching Martian crustal magnetization and magnetic properties of Martian meteorites, *Meteorit. Planet. Sci.*, *40*, 529–540, doi:10.1111/j.1945-5100.2005.tb00961.x.

Sadykov, R. A., N. S. Bezaeva, A. I. Kharkovskiy, P. Rochette, J. Gattacceca, and V. I. Trukhin (2008), Nonmagnetic high pressure cell for magnetic remanence measurements up to 1.5 GPa in a superconducting quantum interference device magnetometer, *Rev. Sci. Instrum.*, *79*, 115102, doi:10.1063/1.2999578.

Sadykov, R. A., N. S. Bezaeva, P. Rochette, J. Gattacceca, S. N. Axenov, and V. I. Trukhin (2009), Nonmagnetic high pressure cell for measurements of weakly magnetic rock samples up to 2 GPa in a superconducting quantum interference device magnetometer, in *Proceedings of the 10th International Conference on Physico-chemical and Petrophysical Investigation in Earth Sciences* [in Russian], pp. 305–306, Division of Earth Sciences of Russian Academy of Sciences, Moscow.

Sato, M., Y. Yamamoto, T. Nishioka, K. Kodama, N. Mochizuki, and H. Tsunakawa (2012), Pressure effect on low-temperature remanence of multidomain magnetite: Change in demagnetization temperature, *Geophys. Res. Lett.*, *39*, L04305, doi:10.1029/2011GL050402.

Searle, C. W. (1967), On the pressure dependence of low-temperature transition in hematite, *Phys. Lett.*, *25A*(3), 256–257.

Sidorov, V. A., and R. A. Sadykov (2005), Hydrostatic limits of Fluorinert liquids used for neutron and transport studies at high pressure, *J. Phys. Condens. Matter*, *17*, S3005, doi:10.1088/0953-8984/17/40/002.

Stöffler, D., K. Keil, and E. R. D. Scott (1991), Shock metamorphism of ordinary chondrites, *Geochim. Cosmochim. Acta*, *55*, 3845–3867.
Umebayashi, H., B. C. Frazer, G. Shirane, and W. B. Daniels (1966), Pressure dependence of the low-temperature magnetic transition in α-Fe_2O_3, *Phys. Lett.*, *22*(4), 407–408.
Vaughan, R. W., and H. G. Drickamer (1967), High-pressure Mossbauer studies on α-Fe_2O_3, $FeTiO_3$, and FaO, *J. Chem. Phys.*, *47*(4), 1530–1536.
Wayne, R. C., and D. H. Anderson (1967), Pressure dependence of the Morin transition in the weak ferromagnet α-Fe_2O_3, *Phys. Rev.*, *155*(2), 496–498.
Wiens, R. C., S. Maurice, and the MSL Science Team (2015), ChemCam: Chemostratigraphy by the first Mars microprobe, *Elements*, *11*, 33–38, doi:10.2113/gselements.11.1.33.
Williamson, D. L., E. L. Venturini, R. A. Graham, and B. Morosin (1986), Morin transition of shock-modified hematite, *Phys. Rev. B*, *34*(3), 1899–1906.
Worlton, T. G., R. B. Bennion, and R. M. Brugger (1967), Pressure dependence of the Morin transition in α-Fe_2O_3 up to 26 kbar, *Phys. Lett.*, *24A*(12), 653–655.
Worlton, T. G., and D. L. Decker (1968), Neutron diffraction study of the magnetic structure of hematite to 41 kbar, *Phys. Rev.*, *171*(2), 596–599.